Endoscopic low-coherence topography measurement for upper airways and hollow samples

Yves Delacrétaz
Etienne Shaffer
Nicolas Pavillon
Ecole Polytechnique Fédérale de Lausanne
CH-1015 Lausanne, Switzerland

Jonas Kühn
University Hospital of Vaud
Site de Cery
CH-1008 Lausanne, Switzerland

Florian Lang
University Hospital of Vaud
ENT Department
Rue du Bugnon 21
CH-1005 Lausanne, Switzerland

Christian Depeursinge
Ecole Polytechnique Fédérale de Lausanne
CH-1015 Lausanne, Switzerland

Abstract. To evaluate the severity of airway pathologies, quantitative dimensioning of airways is of utmost importance. Endoscopic vision gives a projective image and thus no true scaling information can be directly deduced from it. In this article, an approach based on an interferometric setup, a low-coherence laser source and a standard rigid endoscope is presented, and applied to hollow samples measurements. More generally, the use of the low-coherence interferometric setup detailed here could be extended to any other endoscopy-related field of interest, e.g., gastroscopy, arthroscopy and other medical or industrial applications where tri-dimensional topology is required. The setup design with a multiple fibers illumination system is presented. Demonstration of the method ability to operate on biological samples is assessed through measurements on *ex vivo* pig bronchi. © *2010 Society of Photo-Optical Instrumentation Engineers.* [DOI: 10.1117/1.3512218]

1 Introduction

In airways, stenoses treatment mainly consists in laser excision of the pathological process, a dilatation, the placement of an endoluminal prosthesis to keep the airway open, or a combination of these procedures.[1,2] Size of the lumen and length of the stenosis are critical values to determine the appropriate dimensions of the stent to use, thus optimizing chances of recovery.[3]

Quantitative measurements of human upper airways can be performed by either direct or indirect means. Despite being very well implanted in medical facilities and providing accurate results, indirect techniques such as radiology, computed tomography, and magnetic renonance imaging[4,5] are very expensive, time consuming, and more importantly cannot be performed at bedside just before or after an operation. Another possibility is photoacoustic tomography, which provides both structural and functional imaging, and for which comercialized systems are expected soon.[6]

Independent of all radiological developments, endoscopy will remain the gold standard in the preoperative work-up, because nothing will replace direct visual inspection. Since it must be performed in all cases, it seemed logical to develop a way to measure lumen size and stenosis length during this examination. Such direct measurements can be performed with rigid endoscopes, fibroscopes, and with specifically designed probes, as in the optical coherence tomography (OCT) method,[7] and more recently, Fourier domain optical coherence tomography

(FD-OCT),[8,9] which bypasses classical OCT in terms of both speed and signal-to-noise ratio.

Many attempts are reported in the literature based on interferometric methods, such as digital holography (DH) with a multicore fiber,[10] pulsed DH,[11,12] and multi-illumination DH.[13,14] Achievement of miniaturized endoscopic DH by placing the interferometer and detector inside the endoscopic sensor body is also reported.[15] Measurements on porcine stomach by pulsed electronic speckle pattern interferometry (ESPI) has also been demonstrated.[16] Two-wavelength ESPI has been applied to endoscopy,[17] and different studies on the optimization of spatial phase shifting for endoscopic ESPI can be found in the literature.[18]

In low-coherence interferometry, or coherence radar,[19] the envelope of the interference signal is detected, rather than the evaluation of the phase itself. This is usually achieved by calculating the correlation signal of many phase-stepped images, thus providing 3-D contouring, as in Ref. 20, where a five-image algorithm was used. "Coherence gating" techniques have the advantage of providing absolute depth position information, in opposition to phase difference signals that give only relative measurements. The counterpart is that they often require multiple acquisitions to demodulate the signal, preventing "live" recording, unless using rather complicated systems with either multiple sensors or multiple images on the same detector,[21] and fine image registration techniques.

In this work we present a novel technique to obtain endoscopic 3-D contouring of upper airways based on a low-coherence interferometer. The goal is to detect the location of the coherent addition of the object and reference wave on the

Address all correspondence to: Ecole Polytechnique Fédérale de Lausanne (EPFL), Advanced Photonics Laboratory (MVD), CH-1015 Lausanne, Switzerland. Tel: 41-21-69-35-182; Fax: 41-21-39-33-701. E-mail:yves.delacretaz@epfl.ch.

image. With this device, only one acquisition is needed to obtain an absolute contour depth. Usually, interferometric measurements are highly sensitive to phase fluctuations. However, in our case, as the interferometric approach is used to detect whether there is coherent superposition or not, the setup is intrinsically not affected by phase fluctuations between acquisitions. Traditionally, landmarks are placed with a pencil on the scope and then measured and documented on a specially prepared scheme. This approach gives an accuracy of about ± 3 mm. Moreover, the result is dependent on the endoscopist's experience. Our method provides much more accurate results, with a sufficiently robust method to operate under clinical environments.

2 Setup Design

Figure 1 shows a schematic of the device. The setup mainly consists in a smooth reference wave interferometer whose laser source is a low-coherence laser diode, with a coherence length of about 0.3 mm. To illuminate the specimen, a monomode fiber (MF1) is placed in the object arm. Two realizations were investigated to enhance the diameter of the illuminated area: one with a diverging optic adjusted right after the fiber tip, giving access to a field of view with a diameter of 20 mm. This solution has the drawback that the maximum intensity point is situated slightly off-axis, which gives rise to good illumination conditions for one area, but not for all of the observed hollow surface. This asymmetrical configuration showed good results when observing a sidewall, but is not optimal for signal detection on tube-like samples. The retained solution to achieve measurement on the entire circumference of tube-like samples has been to introduce a 1×3 optical coupler after fiber MF1, providing a more symmetrical configuration. Fibers MF11, MF12, and MF13 are equally spaced around the tip of the endoscope, as

depicted in the detailed view in Fig. 1, which gives three illumination zones with their maximal intensity centers located away from the optical axis. Distance between the optical axis of the endoscope and the fibers is chosen so that the illuminated areas do not overlap, assuring that there is no unwanted interference fringes that could potentially result in misleading depth signal extraction.

A beamsplitter (BS) separates the collimated beam (B) generated by the modulated laser diode (LD) into the reference beam and the object beam, which is injected into MF1 and then split in three before illuminating the object (O). A widely available DVD writer laser diode providing a mean power of 15 mW for sample illumination has proven to be an adequate candidate for this setup. The object-scattered light is collected by the endoscope [EN, Karl Storz (Tuttlingen, Germany) 10320A]. With this endoscope, our system has typically a depth of field of 80 mm, with a lateral resolution ranging from 9 cy/mm down to 1.5 cy/mm, depending on the distance between the object and the endoscope tip, with the highest resolution being achieved for objects close to the tip. The reference wave (R) is first directed to a delay stage (DS), which consists of two mirrors (M1 and M2) mounted on a motorized axis. In this way it is possible to adjust the time delay between R and O. The reference wave is then injected in another monomode fiber (MF2) and transmitted to the part of the device attached to the endoscope eyepiece (overall dimensions are $115\times 83\times94$ mm). MF2 also serves as a spatial filter to clean the reference beam. The object wave interferes on the charge-coupled device (CCD) plane with the reference wave projected on the camera through a second beamsplitter. A lens is placed at the end of the reference fiber to match the divergence and the size of the reference and object beam. Another lens (L4) forms on the CCD an image of the object modulated by the interference of R and O. The end of
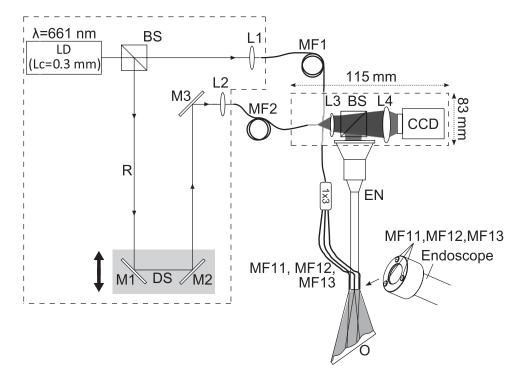

Fig. 1 Schematic of the setup. LD: laser diode. BS: beamsplitter. M1, M2, and M3: mirrors mounted on a motorized translation stage. L1 through L4: lenses. CCD: charged-coupled device camera. EN: rigid endoscope (Karl Storz 10320A). MF: monomode fibers. R: reference wave. O: object.
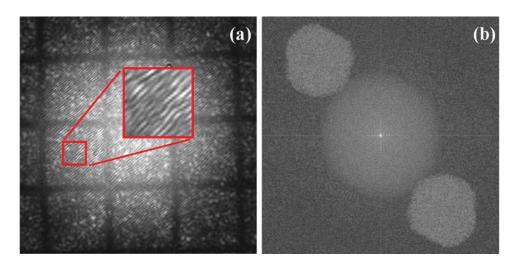
Fig. 2 (a) Typical signal when observing a perpendicular plane made of white paper containing a 2-mm grid. (b) Fourier spectrum of (a).

the reference fiber is placed on an *xy* stage, providing the ability to create adjustable carrier fringes on the interferogram. Carrier fringes will be present only on image points corresponding to an optical path length difference shorter than the coherence length. This fringe pattern delineates a contour depth with a resolution given by the coherence length, and thus the full topography of the specimen under study can be retrieved by varying the time delay between R and O with the DS.

Side viewing with an angled endoscope tip is often used to observe internal organ walls. The presented method would also work with such endoscopes. However, for quantitative measurement of a tube-like object, the full circumference and depth has to be in the field of view, which is hardly possible with side viewing.

3 Detection Algorithm

As in holography, an off-axis configuration creates carrier fringes separating the two image terms (R^*O and RO^*) and the zero-order term ($|O|^2 + |R|^2$).[22] This characteristic can then be used to perform the extraction of the coherent zone on the image in only one acquisition. For a convenient relative distance between the source point of the two spherical waves R and O, the frequencies corresponding to the carrier fringes can be clearly distinguished in the Fourier spectrum, which allows the extraction of the depth information. Figure 2(a) shows a typical interferogram obtained with the endoscopic setup when observing a plane made of white paper containing a 2-mm grid perpendicular to the optical axis, and Fig. 2(b) shows the corresponding Fourier spectrum, where the carrier frequency is clearly observable. It has to be noted that single shot contouring is achievable only if interferometric carrier fringes spatially modulate the speckle. Thus the speckle grains must be at least twice as large as the fringes' periodicity. If the speckle size is smaller than this limit, the detectability of the signal will decrease as well as the measurement accuracy.[23]

Investigations were made to perform detection either in the frequency domain or in the space domain. In the frequency domain, the detection of the coherent zone is based on the calculation of a local spectrum.[23] A sliding window filter is constituted by calculating the fast Fourier transform (FFT) on a neighborhood of 8×8 pixels; the retained output value is then the maximum amplitude of the local spectrum. This method is hereafter denoted as "local FFT." This technique shows good sensitivity, but is quite time consuming (more than 40 s on an Intel Pentium® 4 CPU at 3.4 GHz, for one acquisition).

On the other hand, detection procedures in the space domain are much faster.[24] Using match pattern analysis, a set of well suited filters are calculated, and the convolution between these filters and the acquired image isolates the fringes, thus locating the coherent zone on the image. Tests were achieved with discrete cosine and Gabor filter banks.[25] Discrete cosine filter banks are very fast, as they output only real values, but are about twice less sensitive as Gabor filter banks, which makes them unsuitable for our application. Gabor filter banks output complex values. They are defined with a frequency and an orientation. Calculations are a bit more time consuming (2 s to filter an acquisition versus 1.5 s for discrete cosine filter banks), but are far less than the local FFT approach, and show reasonable sensitivity.[26]

After filtering, the signal is thresholded. To remove the remaining noisy point, we have developed a curve tracking algorithm. Given a pixel neighborhood, the significant points are selected by following the maximum variance.

It is technically difficult and expensive to ensure that MF11, MF12, and MF13 are exactly the same length. Although, if the differences in length of the illumination fibers can be compensated with the delay stage, it can be overcome by a simple calibration procedure and subsequent application of three digital masks. The calibration procedure consists of measuring the illumination fiber length differences, which can be achieved by observing a flat sample while changing the DS position. In our case, the maximal fiber length difference was 4.3 mm. After the calibration procedure, the absolute depth value for each extracted points is known with respect to the position of the DS. Finally, the digital masks are used to map different depths to image areas illuminated with different fibers; the resulting signal is set to zero for object points that are not illuminated with the fiber currently processed. The algorithmic procedure used to retain the significant data points after thresholding is thus applied sequentially to the extracted points corresponding to each illuminated area. After taking into account the lateral
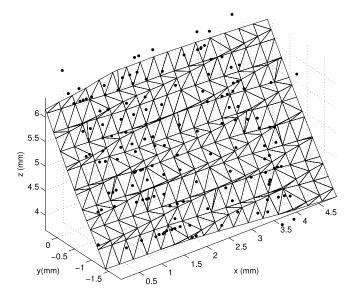
Fig. 3 Validation measurement on a tilted plane. Representation of the measured points (black dots) along with the interpolating surface (mesh).

magnification, which is dependent on the depth value of the extracted point, we obtain three sets of measured 3-D points, each associated with a different depth, for each acquisition.

Finally, to obtain a user interpretable display, a closed surface of the tube-like structure observed is built by interpolating the data points with radial basis function, as described in Ref. 27.

4 Results

Measurements have been made on different samples, such as planar and cylindrical paper shapes and metallic cylinders. Results on *ex-vivo* pig parts, presumed to be highly representative of the signal that will be obtained when observing human upper airways, are also presented.

First, to validate the device setup and the detection algorithm, measurements were made on a tilted plane, as illustrated on Fig. 3, with a field of view of 5 mm. 3-D reconstruction was achieved by scanning with the delay system (see mirrors M1 and M2 on Fig. 1) with steps of 0.2 mm. The sample is made with a sheet of paper, which provides an almost homogeneous diffusive sample with a small mean free path.

Black dots indicate the detected points, repositioned in an *xyz* coordinate system in the object space, along with a surface interpolating the data points (mesh). Several measurements with different tilt values for the plane were performed, and the root mean square error (RMSE) between the real data points and the corresponding points on the fitted surface was calculated each time, showing a mean value of 0.4 mm. The algorithmic procedure does not introduce a significant loss in accuracy, compared to the physical accuracy limit given by the laser source coherence length of 0.3 mm. It has to be noted that, compared to the ±3-mm accuracy obtained with handmade landmarks, the accuracy is at least four times better and independent of any endoscopist's experience.

Figure 4(a) shows measurements on a metallic cylinder obtained with a simplified illumination configuration: only one fiber, attached to the housing of the endoscope, has been used to illuminate the sample. As the numerical aperture of an optical fiber is too small to illuminate the whole object, a 1.5-mm-diam ball lens made of BK7 has been positioned after the fiber end with a custom-made mounting element. Even though the field of view is enhanced with the use of optics, the algorithm fails to extract the signal on the entire circumference. This is due to the fact that the intensity is adequate for points in the vicinity of the optical axis of the illumination fiber, but not high enough for points situated outside this region.

Using three fibers for illumination gives consequently the advantage of distributing the illumination power more homogeneously on the entire field of view. The signal extraction procedure can be used to obtain 3-D information for different points
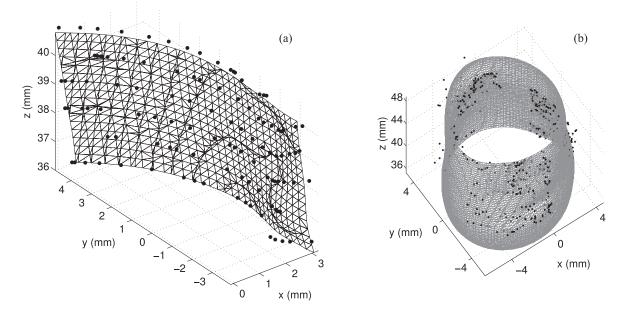

Fig. 4 (a) Measurement on a metallic cylinder. The configuration using a single fiber with a ball lens to extend the illuminated area was used (see text for detailed optical configuration). (b) Measurement on a paper cylinder, using the setup shown in Fig. 1, with three fibers for illumination.
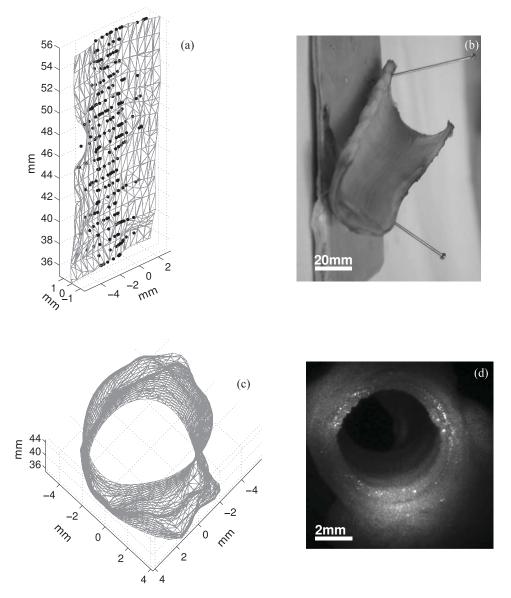
Fig. 5 Pig trachea measured *ex vivo*: (a) final 3-D reconstruction of part of the trachea wall. (b) Picture of the measured *ex-vivo* trachea part. Pig bronchus measured *ex vivo*: (c) final 3-D reconstruction. (d) Usual endoscopic view captured with the system.

on the circonference, allowing us to interpolate a closed surface for a tube-like shape. The fibers are placed in such a way that the three zones are not overlapping, so that it is possible to extract sequentially the signal for each illuminated area. Figure 4(b) presents a measurement made on a 9-mm-diam paper cylinder. The diameter of this cylinder can be considered constant at this measurement scale. However, some deviations from this perfect cylinder can clearly be seen. A root mean square error of 0.7 mm has been evaluated on the measured radius. A possible explaination for the loss in accuracy compared to the measurement on the tilted plane is that the error on the lateral magnification depth dependency, which needs to be taken into account for 3-D positioning of the extracted points, has an impact when measuring the cylinder, and affects the overall accuracy, whereas it is not the case when measuring a tilted plane.

Figure 5(a) shows results obtained on an *ex-vivo* pig trachea sample. The separation between each acquired curve level is 1 mm. The acquisition time is a critical parameter, as the sample

is a dynamic medium. Small deformations of the sample due, for example, to water evaporation at the surface, can produce fringe blurring if the integration time of the CCD is too long, thus preventing curve extraction. We observed that for acquisition times higher than 2 ms, the fringe contrast becomes too low to be detected.

Figure 5(c) shows a measurement obtained on a small *ex-vivo* pig bronchus using three fibers for illumination. Separation between each acquired interferogram is 0.2 mm, which results in data cloud points of 972 tridimensional coordinates. The interpolated surface used for visualization was evaluated on 2240 vertexes. Compared to metallic samples, a source of imprecision on biological samples is related to the light penetrating the sample: part of the photons encounter single scattering. These photons can potentially be backscattered in the direction of the detector, and propagate on the same optical path length as the reference, and thus participate in the interference with the reference wave. Such photons are coming from positions

closer to the endoscope than the one to be isolated, and a wider interference pattern is observed.

5 Conclusion

In contrast with indirect imaging techniques, low-coherence endoscopy allows for measurements directly *in situ*, e.g., within an operating room, and therefore does not require the patient to be moved to an imaging facility. Moreover, it is shown that the use of a low-coherence source in an off-axis configuration interferometer, in conjunction with the inherent small aperture of rigid endoscopes, can be efficiently used to separate the desired signal from the background, either in the Fourier spectrum or by filtering in the space domain with Gabor filters, thus allowing us to acquire the depth information in a single acquisition. Impact of the illumination design on the detectability of the signal is highlighted. A compact solution (overall volume 115×83×94 mm) for the realization of the device is designed, characterized, and tested on an *ex-vivo* pig sample. It demonstrates that our low-coherence endoscope can be successfully used to obtain tridimensional imaging of upper airways.

References

1. C. Bolliger, T. Sutedja, J. Strausz, and L. Freitag, "Therapeutic bronchoscopy with immediate effect: laser, electrocautery, argon plasma coagulation and stents," *Eur. Respir. J.* **27**, 1258–1271 (2006) ISSN 09031936.
2. J. Dumon, "A dedicated tracheobronchial stent," *Chest* **97**, 328–332 (1990).
3. G. Simpson, M. Strong, G. Healy, S. Shapshay, and C. Vaughan, "Predictive factors of success or failure in the endoscopic management of laryngeal and tracheal stenosis," *Ann. Otol. Rhinol. Laryngol.* **91**, 384–388 (1982).
4. S. Nemec, C. Krestan, I. Noebauer-Huhmann, M. Formanek, J. Frühwald, P. Peloschek, F. Kainberger, and C. Czerny, "Radiological normal anatomy of the larynx and pharynx and imaging techniques," *Radiol. Normal. Larynx Pharynx Sowie Bildgebende Tech. Radiologe* **49**, 8–16 (2009) ISSN 0033832X.
5. H. Eslamy and B. Newman, "Imaging of the pediatric airway," *Paediatr. Anaesth.* **19**, 9–23 (2009) ISSN 11555645.
6. C. Li and L. Wang, "Photoacoustic tomography and sensing in biomedicine," *Phys. Med. Biol.* **54**, R59–R97 (2009).
7. J. J. Armstrong, M. S. Leigh, I. D. Walton, A. V. Zvyagin, S. A. Alexandrov, S. Schwer, D. D. Sampson, D. R. Hillman, and P. R. Eastwood, "In vivo size and shape measurement of the human upper airway using endoscopic long-range optical coherence tomography," *Opt. Express* **11**, 1817–1826 (2003).
8. L. Froehly, S. N. Martin, T. Lasser, C. Depeursinge, and F. Lang, "Multiplexed 3d imaging using wavelength encoded spectral interferometry: a proof of principle," *Opt. Commun.* **222**, 127–136 (2003).
9. A. Tumlinson, J. Barton, B. Povazay, H. Sattman, A. Unterhuber, R. Leitgeb, and W. Drexler, "Endoscope-tip interferometer for ultrahigh resolution frequency domain optical coherence tomography in mouse colon," *Opt. Express* **14**, 1878–1887 (2006).
10. O. Coquoz, R. Conde, F. Taleblou, and C. Depeursinge, "Performances of endoscopic holography with a multicore optical fiber," *Appl. Opt.* **34**, 7186–7193 (1995).
11. G. Pedrini, M. Gusev, S. Schedin, and H. J. Tiziani, "Pulsed digital holographic inter-ferometry by using a flexible fiber endoscope," *Recent Develop. Digital Speckle Patt. Interferom. Opt. Lasers Eng.* **40**, 487–499 (2003).
12. S. Schedin, G. Pedrini, H. J. Tiziani, and A. K. Aggarwal, "Comparative study of various endoscopes for pulsed digital holographic interferometry," *Appl. Opt.* **40**, 2692–2697 (2001).
13. T. S. Anaya, F. M. Santoyo, M. DeLaTorre-Ibarra, G. Pedrini, and W. Osten, "Endoscopic pulsed digital holography for 3d measurements," *Opt. Express* **14**, 1468–1475 (2006).
14. T. S. Anaya, M. D. la Torre, and F. M. Santoyo, "Microstrain detection using simultaneous endoscopic pulsed digital holography," *Opt. Eng.* **47**, 073601 (2008).
15. E. Kolenovic, W. Osten, R. Klattenhoff, S. Lai, C. von Kopylow, and W. Ju¨ptner, "Miniaturized digital holography sensor for distal three-dimensional endoscopy," *Appl. Opt.* **42**, 5167–5172 (2003).
16. B. Kemper, D. Dirksen, W. Avenhaus, A. Merker, and G. VonBally, "Endoscopic double-pulse electronic-speckle-pattern interferometer for technical and medical intracavity inspection," *Appl. Opt.* **39**, 3899–3905 (2000).
17. J. Kandulla, B. Kemper, S. Knoche, and G. VonBally, "Two-wavelength method for endoscopic shape measurement by spatial phase-shifting speckle-interferometry," *Appl. Opt.* **43**, 5429–5437 (2004).
18. B. Kemper, J. Kandulla, D. Dirksen, and G. von Bally, "Optimization of spatial phase shifting in endoscopic electronic speckle pattern interferometry," *Opt. Commun.* **217**, 151–160 (2003).
19. T. Dresel, G. Häusler, and H. Venzke, "Three-dimensional sensing of rough surfaces by coherence radar," *Appl. Opt.* **31**, 919–925 (1992).
20. I. Balboa, H. D. Ford, and R. P. Tatam, "Low-coherence optical fibre speckle interferometry," *Measure. Sci. Technol.* **17**, 605–616 (2006).
21. M. S. Hrebesh, Y. Watanabe, and M. Sato, "Profilometry with compact single-shot low-coherence time-domain interferometry," *Opt. Commun.* **281**, 4566–4571 (2008).
22. E. Cuche, P. Marquet, and C. Depeursinge, "Simultaneous amplitude-contrast and quantitative phase-contrast microscopy by numerical reconstruction of fresnel off-axis holograms," *Appl. Opt.* **38**, 6994–7001 (1999).
23. Y. Delacrétaz, N. Pavillon, F. Lang, and C. Depeursinge, "Off-axis low coherence inter-ferometry contouring," *Opt. Commun.* **282**, 4595–4601 (2009).
24. M. Unser, "Local linear transforms for texture measurements," *Signal Process.* **11**, 61–78 (1986).
25. I. Kalliomäki and J. Lampinen, "On steerability of gabor-type filters for feature detection," *Patt. Recog. Lett.* **28**, 904–911 (2007) ISSN 0167–8655.
26. T. Randen and J. Husoy, "Filtering for texture classification: a comparative study," *IEEE Trans Patt. Anal. Mach. Intell.* **21**, 291–310 (1999).
27. J. Carr, W. Richard Fright, and R. Beatson, "Surface interpolation with radial basis functions for medical imaging," *IEEE Trans. Med. Imag.* **16**, 96–107 (1997).